Systematics of dynamic moment of inertia in super-deformed bands in Mass ∼150 region

S. Roy

Department of Nuclear and Atomic Physics,

Tata Institute of Fundamental Research, Mumbai- 400 005, India

arXiv:1605.07295v2 [nucl-th] 29 Jun 2016

Abstract

An empirical semi-classical model have been proposed to investigate the nature of dynamic moment-of-inertia , of the super-deformed (SD) bands in nuclei of mass 150 region. The model incorporates an additional frequency dependent distortion, to the dynamic moment-of-inertia term akin to a vibrational component to explain the extreme spin structure of these bands. Using this model two separate components to the dynamic moment of inertia, $\Im^{(2)}$ have been identified for the SD band structure for the mass 150 region. Three distinct nature of the moment-of-inertia, also have been identified using the two parameter model.

PACS numbers:

Keywords: super-deformation, A=150, semi-classical model

I. INTRODUCTION

The super-deformation in atomic nuclei has been an exhaustively studied intriguing high spin phenomenon. Till date, more than three hundred super-deformed (SD) bands have been reported across the mass regions [1]. The super-deformation in a nucleus have been characterized by an extended ellipsoidal shape, that may be imagined as a rugby ball. For the ideal SD case the ellipsoidal long axis is twice the short axis in length, and corresponds to a quadrupole deformation, of $\beta \sim 0.6$ [2]. Such an extended shape is stable at high spin and rotational frequency due to the interplay of collective and single particle degrees of freedom. The primary factors for the stability of shape is due to the shell corrections, which produces a local minima in the potential-energy-surface, and the decrease of the Coulomb force due to larger than average separation of protons. In addition, at this high spin range ($I \geq 30\hbar$), presence of highly mixed j-states presents an interesting domain for theoretical studies. There has been many exhaustive theoretical studies, using mean field models; Woods-Saxon [3], anharmonic oscillator potential [4, 5], and Skyrme-Hartree-Fock [6]. Quite a few semi-classical macroscopic models are has also been successful in presenting a good description of the SD bands [7–11].

In the super-deformation regime, the nucleus exhibits nearly a perfect quadrupole behaviour, with a very small regular separation in the rotational level energies. This feature may manifests as identical SD bands in neighbouring nuclei [13] due to similar moment-of-inertia. Certain features of the moment-of-inertia has also been studied by the semi-classical model, where a stiff core part was identified at high spin (Eq. 1) [7].

$$\Im = \frac{3}{4}\Im_{rigid} + \frac{1}{4}\Im_{irrotational} \tag{1}$$

where, $\Im_{rigid}$ and $\Im_{irrotational}$, are the respective rigid-core and irrotational contribution to the total moment-of-inertia, $\Im$ [7].

Characteristics of a rotational band can be investigated, from the energy of the levels (E_L) and the angular momentum (I). The moment-of-inertia ($\Im$), kinematic-moment-of-inertia ($\Im^{(1)}$) and dynamic-moment-of-inertia ($\Im^{(2)}$), here after also referred to as D^{MOI}, are the three quantities that defines the evolution of the band with the spin. These are given

by,

$$\Im^{(1)} = I\left(\frac{dE}{dI}\right)^{-1}$$
$$\Im^{(2)} = \left(\frac{d^2E}{dI^2}\right)^{-1} \tag{2}$$

For an ideal rotor, $\Im \equiv \Im^{(1)} \equiv \Im^{(2)}$. However, in a realistic scenario, the excited levels in a nucleus have also been determined by pairing effect between the valance nucleons and the centrifugal stretching due to rotation [6]. Both the effects results in a D^{MOI} that is dependent on the rotational frequency.

For a deformed nucleus in which the spheroidal collective field is cranked about a fixed axis, a general expression for moment-of-inertia was given by, A. Bohr, B. R. Mottelson, S. A. Moszkowski and D. R Inglis [14–16],

$$\Im_{Inglis} = \frac{\hbar}{\omega_2\omega_3}\left[\frac{(\omega_2-\omega_3)^2}{\omega_2+\omega_3}\sum(m+n+l) + \frac{(\omega_2+\omega_3)^2}{\omega_2-\omega_3}\sum(n-m)\right] \tag{3}$$

where, l, m, and n are the oscillator quantum number in the three dimensions defining the single nucleon states, ω_2 is the oscillator frequency in x and y direction and ω_3 is the oscillator frequency in the z direction. For $\omega_2 \neq \omega_3$ $\sum(n-m)$ is zero. The first term is associated with the irrotational-flow for distorted closed shell which has been shown to have a substantial contribution to the nature of D^{MOI}. In addition, the angular frequency, ω associated with such a motion has been give by,

$$\omega^2 = \omega_2^2[1 \pm 4\Omega^2/(\omega_2^2 - \omega_3^2)] \tag{4}$$

where, Ω is the angular velocity of the cranking of the nucleus about a fixed axis. At this juncture, one wonders if such a framework coupled with the previously mentioned formalism (Eq. 1), could be used to directly to investigate the moment-of-inertia of the SD bands.

Interestingly, a simple semi-classical expression between $\Im^{(1)}$ and $\Im^{(2)}$ has been derived by C. S. Wu *et al.,* [10–12]. The two parameter expression, using the Bohr Hamiltonian for a well deformed nucleus with small axial symmetry has been quite successful in describing SD band rotational spectrum. Here the authors have quantified a constant R an a function of the angular momentum I, such that $R \equiv \sqrt{[\Im^{(1)}]^3/\Im^{(2)}}$. One can infer from this formalism,

that the moment of inertia can be represented in a functional form $f_n(\omega)$, $n = 1$ and $n = 2$, gives, $\Im^{(1)}$ and $\Im^{(2)}$, respectively. The function is given as,

$$f_n(\omega) = \Im_\circ \left[1 - \frac{(\hbar\omega)^2}{a^2 b}\right]^{(\frac{1}{2}-n)} \tag{5}$$

where, $\Im_\circ$, is the band-head moment of inertia, $\Im_\circ$, and a, and b are related with $\Im_\circ$ via,

$$\Im_\circ = \frac{\hbar^2}{ab} \tag{6}$$

The preceding two equations, 5 and 6, indicates that the there is slow variation of D^{MOI} with rotational frequency. In addition, the dynamic- and kinematic- moment of inertia in SD bands are related to the bandhead moment-of-inertia, $\Im_\circ$ through the two parameters, and rotational frequency, ω, as the independent variable (Eq. 5, Eq. 6).

In our proposed model, the primary motivation of the three semi-classical scenarios mentioned previously, have been put together. With this model the dynamic-moment-of-inertia, $\Im^{(2)}$, as a function of rotational frequency have been investigated. The model is chosen, such that it incorporates a vibration-like distortion part and describes the slow variation of D^{MOI} for certain SD bands where there is no sudden alignment. The function has the property such that, at the bandhead the magnitude of the vibrational coupling is maximum and it goes to zero at the maximum observed spin ω_{max}.

D^{MOI} as a function of rotational frequency and vibration distortion is given by,

$$\Im^{(2)} = \Im_c^{(2)} \pm \Im_\chi^{(2)} \left[\frac{\omega_{max} - \omega}{\omega_{max}}\right]^2 \tag{7}$$

where, $\Im_c^{(2)}$, and $\Im_\chi^{(2)}$, are, respectively, the constant and the variational part of D^{MOI}. Parameter $\Im_\chi^{(2)}$ is such that it describes the magnitude of deviation of D^{MOI} from a perfect rotor. The quantity $((\omega_{max} - \omega)/\omega_{max})^2$ is a function of rotational frequency, ω, such that at $\omega = \omega_{max}$, it goes to zero. Depending on the initial curvature of the experimental D^{MOI}, the coupling between $\Im_c^{(2)}$ and $\Im_\chi^{(2)}$ is either positive or negative. $\Im_\chi^{(2)}$ couples positively to the constant part, if the vibration is in the plane of rotation. For the negative coupling, the vibration is more aligned towards the rotation axis.

II. FORMALISM

The atomic nucleus is a finite Fermi system. The value of moment of inertia of the nucleus $\Im$, lies between a rigid rotor and a liquid rotor, $\Im_{liquid} < \Im < \Im_{rigid}$. One can extract

the moment of inertia parameter for rotational band using the relation, $E_x = \frac{\hbar^2}{2\Im} I(I+1)$. However, the average properties of a band in a nucleus are better described by the $\Im^{(1)}$, and D^{MOI}.

Experimentally, for most of the SD bands the bandhead spin is not assigned firmly, due to the missing or low intensity of the intra-band linking transitions. So, in this work the properties of SD bands have been viewed from the D^{MOI} perspective, and the global patterns in the mass region 150 are observed.

The D^{MOI} function is given as in Eq. 7. The function is single valued and smooth. The function has a constant part $\Im_c^{(2)}$ and a slowly varying angular frequency dependent part, parametrized through $\Im_\chi^{(2)}[(\omega_{max}-\omega)/\omega_{max}]^2$. Using least-square fitting the two parameters of this function were extracted from the experimental D^{MOI} values. Then constant part is related to the MOI of the rigid core and the variation part is similar to first term of Inglis moment of inertia $\Im_{Inglis}$ [16].

In this model the vibrational distortion effect is parametrized through the effective moment-of-inertia, $\Im_\chi$ as a function of rotational frequency. It is noteworthy that the function is a constant, if ω is scaled to $[(\omega_{max}-\omega)/\omega_{max}]^2$.

III. RESULTS

The D^{MOI} (Eq. 7), have been fitted to the experimental values using least square minimum procedure to extract the two parameters, $\Im_c^{(2)}$, and $\Im_\chi^{(2)}$. The extracted values are tabulated in Table I, along with the RMS of the residuals for the fit, $\sum_{i=1}^{n}(\Im_i^{(2)_{cal}} - \Im_i^{(2)_{obs}})^2/n$, where n, $\Im^{(2)_{cal}}$, and $\Im^{(2)_{obs}}$ respectively, are the number of data points, calculated value of D^{MOI} and observed value of D^{MOI}. For each of the twenty five cases shown here, the nature of the D^{MOI} in the entire rotational frequency range is reproduced quite well.

While, the experimental values of the constant part to D^{MOI}, $\Im_c^{(2)}$, has a small spread, $72.3^{+15.2\%}_{-9.36\%}$, the $\Im_\chi^{(2)}$ values span 3.7 $\hbar^2\mathrm{MeV}^{-1}$ to 88.7 $\hbar^2\mathrm{MeV}^{-1}$. The characteristics of D^{MOI} have been identified through the magnitude and coupling (positive or negative) of the parameter $\Im_\chi$.

In the figures 1, 2, and 3, the nuclei with three distinct patterns in D^{MOI} components are plotted. Three categories of D^{MOI}, **I**, **II**, and **III**, are identified depending on the magnitude of the ratio of the D^{MOI} component, $\Im_c^{(2)}$ and $\Im_\chi^{(2)}$ and nature of the coupling.

In the category **I**, the average magnitude of $\Im_c^{(2)}$ is about eight times the average magnitude of $\Im_\chi^{(2)}$ (Fig. 1). The nuclei, ^{143}Eu, band 1, ^{143}Gd yrast SD band, ^{144}Gd band 2, and, ^{147}Tb yrast SD band, fall under this category. In this region two other SD bands, ^{150}Tb SD band 2, and ^{151}Dy SD band 1 also show similar magnitude of the negative coupling of $\Im_\chi^{(2)}$, but the magnitude of $\Im_c^{(2)}$ is quite higher and hence not included in the category **I**.

Thus, the region **I** is characterized by the averages $\Im_c^{(2)} = 68.7$ ($\hbar^2\ MeV^{-1}$)), and $\Im_\chi = 8.8$ ($\hbar^2\ MeV^{-1}$). Curiously, the coupling between the D^{MOI} component is negative, hence, the initial D^{MOI} starts with a lower value, that gradually increases and becomes equal to $\Im_c$ at $\omega = \omega_{max}$. The shaded blue region in the figure 1 corresponds to $\pm 5\%$ of the average values, depicted by the red line. All the experimental $\Im^{(2)}$ values are found to be within the region.

In the category **II** (Fig. 2), the coupling between $\Im_c^{(2)}$ and $\Im_\chi^{(2)}$ is positive, and average value of the D^{MOI} components are $\Im_c^{(2)} = 82.98$ ($\hbar^2\ MeV^{-1}$) , and $\Im_\chi^{(2)} = 17.1$ ($\hbar^2\ MeV^{-1}$). Here, $\Im_c^{(2)}$ is higher than other two region and about five times the average $\Im_\chi^{(2)}$ value. As a result of the coupling the initial D^{MOI} is higher and decreases to $\Im_c^{(2)}$ value at $\omega = \omega_{max}$. ^{150}Gd SD band 12, ^{151}Tb SD band 2, ^{152}Dy SD band 1, and ^{153}Dy SD band 3 belong to this category. The green region represents the $\pm 5\%$ of the average values shown by the red line.

In the final category, **III**, we have thirteen bands, where $\Im_c^{(2)}$ is about 1.5 times $\Im_\chi^{(2)}$ and the coupling is positive like the previous category. Due to considerable increase in the magnitude of the frequency dependent part, the initial D^{MOI} is high and decreases much rapidly than the other two categories. The D^{MOI}, components $\Im_c^{(2)}$ and $\Im_\chi^{(2)}$ have comparable magnitude and on the average are given as, 69.3 ($\hbar^2\ MeV^{-1}$) and 47 ($\hbar^2\ MeV^{-1}$), respectively.

IV. SUMMARY

A empirical semi-classical two parameter model have been used to investigate the characteristics of D^{MOI} of SD band in mass 150 region. Using the model three categories of D^{MOI} have been identified. The D^{MOI} in this model have been parametrized such that, the component $\Im_c^{(2)}$ is constant and $\Im_\chi^{(2)}$ is dependent on angular frequency. Experimental values, of twenty five SD bands, which show a smooth behaviour have been fitted using the equation 7. In all the cases we have a reasonably good fit.

The three categories of the D^{MOI}, are shown for a given angular frequency range figure 4. It is interesting to note that at the lower frequency limit, category **II** and category **III**, D^{MOI} overlap. This indicates that in both the scenario, the bandhead D^{MOI} is similar, but the coupling of the angular frequency dependent component is different. At higher angular frequency, these two DMOI become distinctly separate and reach the respective average rigid core values of 82.98 ($\hbar^2\ MeV^{-1}$) and 69.3 ($\hbar^2\ MeV^{-1}$) for category **III** and category **II**.

At the higher frequency limit, D^{MOI} category **I** and **II** overlap. The coupling of $\Im_{\chi}^{(2)}$ is negative and this results in a lower D^{MOI} at the bandhead. At the higher frequency the this effect diminishes and two category of D^{MOI} **II** and **I** merges to the average value of ~ 69 ($\hbar^2\ MeV^{-1}$).

In this study three distinct patterns of the D^{MOI} have been highlighted. A substantial number of SD bands have been treated using the model and good agreement is observed between the experiment and theory. As a result, the D^{MOI} may be thought to have a rather weak dependence on their respective nucleonic configurations. The angular frequency component given by, $[(\omega_{max} - \omega)/\omega_{max}]^2$, is a direct measure of the distortion effect and responsible for the deviation from the ideal rotor. It is natural that this model will also work for smooth SD bands in other mass region. The present model can also be extended to calculate the B(E2) rates, by parametrizing the charge asymmetry through the distortion effect.

V. ACKNOWLEDGEMENT

Discussions with R. G. Pillay have been very constructive in the preparation of this manuscript and his insight on the subject matter has been very helpful.

[1] B. Singh *et al.*, Nuclear Data Sheets **97**, issue 2, pages 241 - 592 (2002)

[2] P. J. Twin and P. J. Twin, Ann. Rev. Nucl. Part. Sci. **38**, 533 (1988)

[3] J. Dudek, W. Nazarewicz, Phy. Rev, C **31** 298 (1985)

[4] I. Ragnarsson, Nucl. Phys. A **347**, 287 (1980)

[5] R. Bengtsson, Phys.Scr. **24**, 200 (1981)

[6] W. Satua, *et al.,* Phys. Rev. Lett. **77** 5182 (1996)

[7] W. J. Swiatecki, Phys. Rev. Lett. **58**, 1184 (1987)

[8] S. M. Harris, Phy. Rev. **138**, No. 3B 509 (1965)

[9] J. L. Wood, and R. W. Fink Nucl. Phys. **A224**, 589 (1974)

[10] C. S. Wu and J. Y. Meng, Commun. Theor. Phys.(Beijing) **8**, 57 (1987)

[11] C. S Wu, Phys. Rev. C **45**, number 5, 1992

[12] A. Bohr and B.R. Mottelson, Nuclear Structure, **II**, 591, New York, Benjamin (1975)

[13] C. Baktash, B Haas, and W Nazarewicz, Ann. Rev. Nucl. Part. Sci. **45**, 485 (1995)

[14] A. Bohr and B. R. Mottelson, Kgl. Danske Videllskab. Selskab, Mat. -fys. Medd. **30**, No. 1 (1955).

[15] S. A. Moszkowski, Phys. Rev. **103**, 1328 (1956)

[16] D. R. Inglis Phys. Rev. i**103**, number 8 (1956).

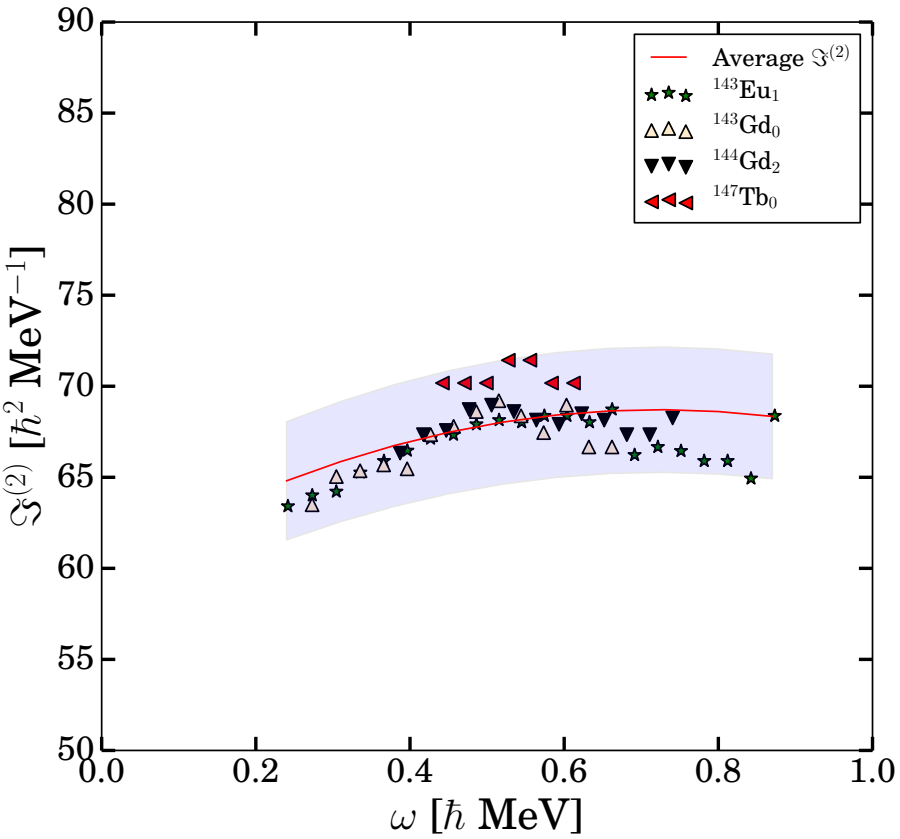

FIG. 1: Category **I**, $\Im^{(2)}$ vs. ω for ^{143}Eu SD band 1, ^{143}Gd SD band, ^{144}Gd SD band 2 and ^{147}Tb SD band are shown. The red line represents the average curve with the parameter value, $\Im_c^{(2)} = 68.7$ ($\hbar^2\ MeV^{-1}$) and $\Im_\chi^{(2)} = 8.8$, respectively. The blue region spans $\pm 5\%$ of the value of the two parameters.

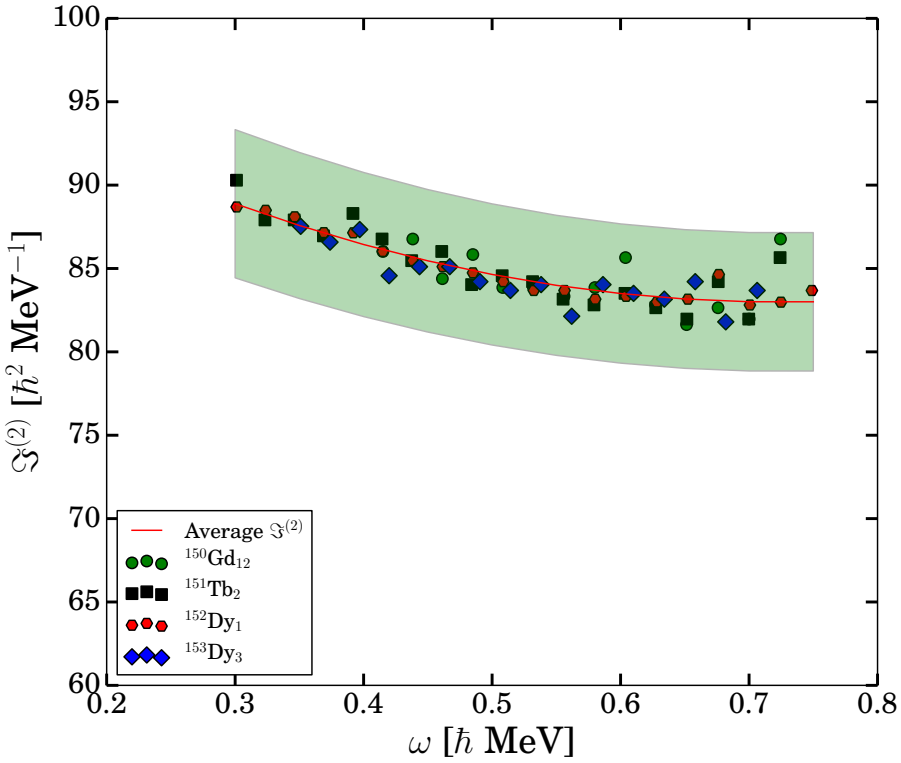

FIG. 2: Category **III**, $\Im^{(2)}$ vs. ω for ^{150}Gd SD band 12, ^{151}Tb SD band 2, ^{152}Dy SD band 1 and ^{153}Dy SD band 3 are shown. The red line represents the average curve with the parameter value, $\Im_c^{(2)} = 82.98$ ($\hbar^2\ MeV^{-1}$) and $\Im_\chi^{(2)} = 17.13$ ($\hbar^2\ MeV^{-1}$), respectively. The green region spans $\pm 5\%$ of the value of the two parameters.

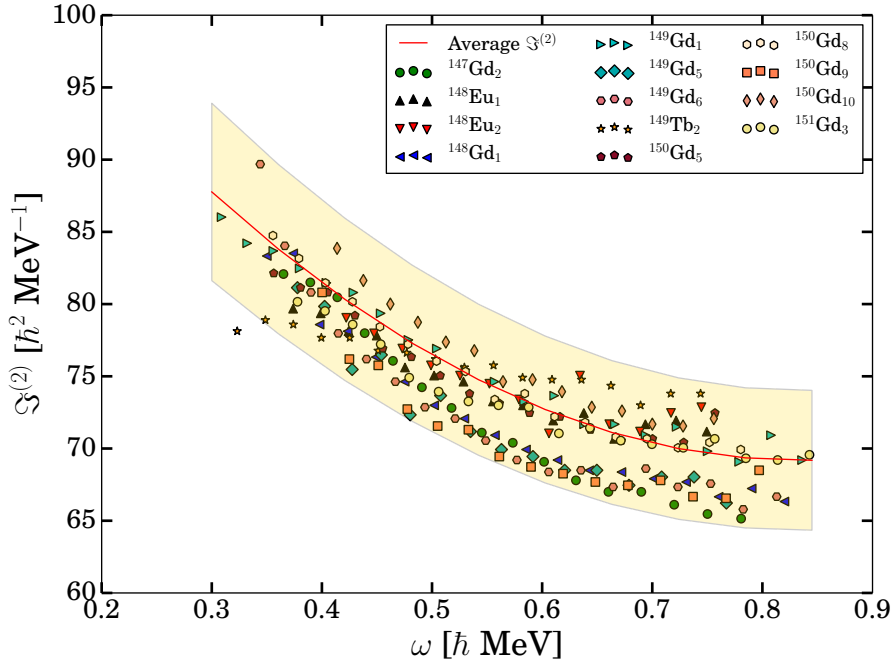

FIG. 3: Category **III**, $\Im^{(2)}$ vs. ω for ^{147}Gd SD band 2, ^{148}Eu SD band 1, ^{148}Eu SD band 2, ^{148}Gd SD band 1, ^{149}Gd SD band 1,^{149}Gd SD band 5, ^{149}Gd SD band 6, ^{149}Tb SD band 2, ^{150}Gd SD band 5, ^{150}Gd SD band 8, ^{150}Gd SD band 9, ^{150}Gd SD band 10, and ^{151}Gd SD band 3. The red line represents the average curve with the parameter value, $\Im_c^{(2)} = 69.18$ ($\hbar^2\ MeV^{-1}$) and $\Im_\chi^{(2)} = 45.21$ ($\hbar^2\ MeV^{-1}$), respectively. The yellow region spans $\pm 7\%$ of the value of the two parameters.

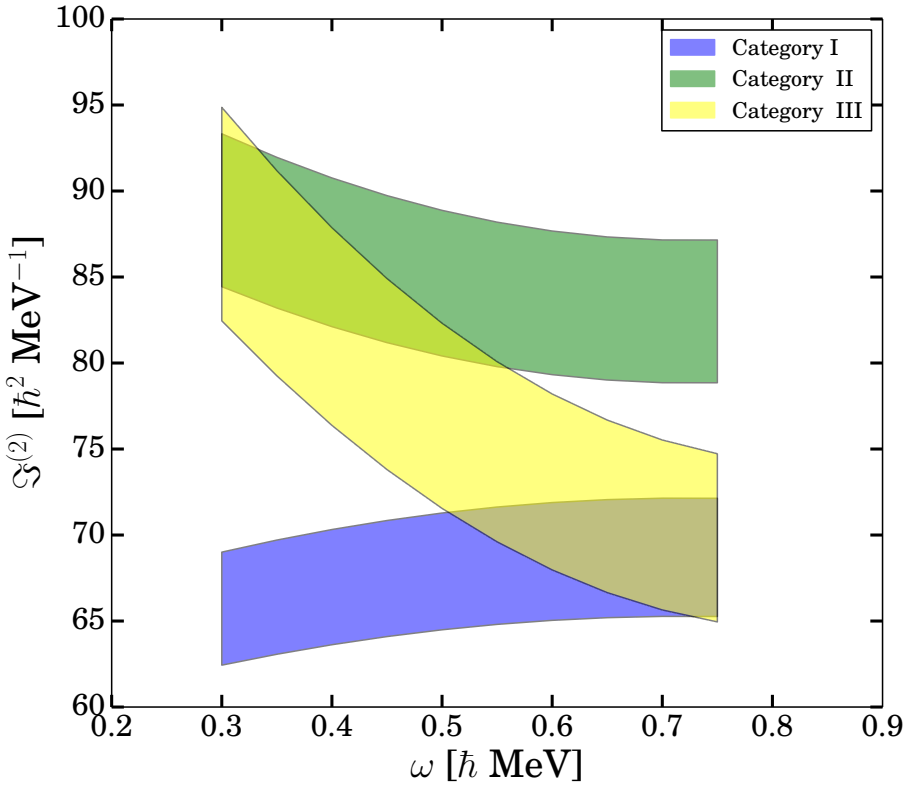

FIG. 4: The $\Im^{(2)}$ vs. ω plot shows the three regions with $\Im_c^{(2)}/\Im_\chi^{(2)} \sim 8$ (blue), $\Im_c^{(2)}/\Im_\chi^{(2)} \sim 5$ (green), and $\Im_c^{(2)}/\Im_\chi^{(2)} \sim 1.5$ (yellow) for the given span of angular frequency.

TABLE I: Fitted parameter values, $\Im^{(2)}_{\circ}$, $\Im\chi^{(2)}$ using the Eq. 7 are tabulated.

Isotope(Band)	$\Im^{(2)}_{\circ}$	$\Im\chi^{(2)}$	rms of residuals
^{143}Eu(SD1)	67.4882	5.51486	1.30959
^{143}Gd(SD)	68.2859	12.0957	1.00398
^{144}Gd(SD2)	68.2249	3.6832	0.703386
^{147}Gd(SD2)	65.6736	62.4044	0.515283
^{147}Tb(SD)	70.8534	13.7481	0.638003
^{148}Eu(SD1)	71.209	35.9854	0.521523
^{148}Eu(SD2)	71.8992	37.1367	1.07683
^{148}Gd(SD1)	66.3205	50.523	0.817359
^{148}Gd(SD6)	70.5666	70.2551	0.617295
^{149}Gd(SD1)	69.9208	41.7947	0.621519
^{149}Gd(SD5)	66.8639	52.4335	0.99385
^{149}Gd(SD6)	65.5212	58.6527	1.71442
^{149}Tb(SD2)	74.1203	16.4275	0.546993
^{150}Gd(SD5)	70.6088	42.7737	0.667379
^{150}Gd(SD8)	70.0014	49.3173	0.307386
^{150}Gd(SD9)	66.3469	47.9009	1.18063
^{150}Gd(SD10)	71.6982	56.9163	0.37468
^{150}Gd(SD12)	83.2367	15.7484	1.48063
^{150}Tb(SD1)	73.4802	17.9999	0.57067
^{150}Tb(SD2)	77.2242	13.5021	1.26347
^{151}Dy(SD1)	79.5679	7.71123	1.51678
^{151}Gd(SD3)	69.2381	35.52	0.594611
^{151}Tb(SD2)	82.8791	19.2366	1.03616
^{152}Dy(SD1)	82.906	16.4917	0.523973
^{153}Dy(SD3)	82.91	17.0606	0.812715